Meccanica (2015) 50:649–664
DOI 10.1007/s11012-014-0010-2

Experimental and numerical analysis of frictional contact scenarios: from macro stick–slip to continuous sliding

Davide Tonazzi · Francesco Massi · Laurent Baillet · Antonio Culla · Mariano Di Bartolomeo · Yves Berthier

Received: 15 February 2014 / Accepted: 24 June 2014 / Published online: 8 July 2014

Abstract This work is an in-depth analysis of frictional phenomena including macroscopic stick–slip and mode coupling instabilities, which can occur at different scales ranging from earthquakes to vibrational issues in machining processes. The paper presents a comparison between experimental observations of frictional macroscopic behaviours reproduced in a dedicated laboratory set-up and numerical simulations, obtained by transient finite element simulations able to reproduce the contact dynamics. The explicit finite element code PLASTD has been used to perform numerical transient analysis of two elastic bodies in frictional contact. On the other hand an experimental set-up has been used to investigate the macroscopic response of two blocks of polycarbonate in relative motion, highlighting how the contact frictional behaviour is affected by the imposed boundary conditions. Time evolution of global contact forces has been investigated; macroscopic stick–slip, modal instability behaviours and the transition to continuous sliding as a function of the system parameters have been observed. The frequency and time analysis of experimental phenomena exhibits a good agreement with numerical results obtained through transient contact simulations. The numerical analysis allows for explaining the interaction between local contact behaviour and system dynamics, which is at the origin of the different frictional scenarios. Maps of the instability scenarios are drawn as a function of boundary conditions or system parameters.

Keywords Frictional scenarios · Stick–slip instability · Mode coupling instability · Continuous sliding · Rupture propagation

D. Tonazzi (✉) · F. Massi · A. Culla · M. Di Bartolomeo
DIMA, Department of Mechanical and Aerospace Engineering, ''La Sapienza'' University of Rome, via Eudossiana 18, 00184 Rome, Italy
e-mail: davide.tonazzi@uniroma1.it

F. Massi
e-mail: francesco.massi@uniroma1.it

A. Culla
e-mail: antonio.culla@uniroma1.it

M. Di Bartolomeo
e-mail: mariano.dibartolomeo@uniroma1.it

D. Tonazzi · Y. Berthier
LaMCoS, Contacts and Structural Mechanics Laboratory, Université de Lyon, CNRS, INSA Lyon, UMR 5259, 20 rue des Sciences, 69621 Villeurbanne, France
e-mail: yves.berthier@insa-lyon.fr

L. Baillet
Institut des Sciences de la Terre (ISTerre), CNRS, Joseph Fourier University, Grenoble 1381 rue de la Piscine, Domaine universitaire, 38400 St. Martin D'Heres, France
e-mail: laurent.baillet@iuf-grenoble.fr

1 Introduction

Contact instability phenomena can lead, with respect to the system parameters (friction coefficient, material damping, sliding velocity, contact pressure, material properties, etc.), to strong system oscillations, discontinuous motion and fastidious noise.

Some recent papers dealt with the frictional dynamics by means of frictional models characterized by few degrees of freedom and rigid/deformable contact behaviour [1, 2]. This kind of modelling is useful to better investigate global non-linear dynamics of the system without accounting for local contact dynamics (wear, plasticity, third body [3], local impact [4]) by means of specific contact law or constitutive interface model [5].

In recent years the local dynamics of frictional contacts and its interaction with the global behaviour of the system has been the subject of experimental and numerical works [6–9].

Frictional contact dynamics is of major interest to several disciplines as tribology, earth science, vibrational mechanics and fracture mechanics. Furthermore, understanding the physical mechanisms that drive the onset of sliding is of great importance to many research and industrial applications such as disk brake squeal [10–13], hip endoprosthesis vibrations [14], wheel rail noise emission [15], machining tool vibrations, earthquakes [6, 16], etc. Recent experimental works [7] focused the attention on the effect of the local dynamics [17] at the contact interface, observing [18] the evolution of precursors (interface rupture fronts) that propagate [19] at different velocities at the onset of sliding. On the other hand numerical works [18, 20, 21] showed how the local interface dynamics (rupture and wave propagation) affects the macroscopic frictional behaviour of the system. In this context the approach commonly adopted in seismology issues to follow the waves generated at the contact interface [22, 23] is coupled with the structural dynamic analysis of the mechanical system. Simulation results [19] show that the coupling between the local contact behaviour at interface (local dynamics) and the global dynamics of the system can induce different macroscopic frictional instability scenarios. By varying a system parameter, the macroscopic frictional dynamics can be characterized by macro stick–slip phenomena, harmonic vibrations due to the mode coupling instability [2, 24], or stable continuous sliding. The macro stick–slip regime is characterized by sudden friction force drops (sliding state) along the time, separated by periods of elastic energy accumulation (stick state). Instead, the modal dynamic instability can occur when a vibration mode of the mechanical system becomes unstable, due to frictional contact forces. Any mechanical system with frictional can generate harmonic acoustic emission (at the frequency of unstable mode) during the relative motion.

The numerical results in [18, 19] highlight how the local phenomena (rupture and wave propagation) generated during the relative motion of the elastic bodies are directly related to the macroscopic response of the system (macro stick–slip, mode coupling, continuous sliding,…). Thus, the frictional behaviour is not exclusively a property of the materials in contact but it's a more complex process, which needs to consider the interaction between the interface dynamics and the system structural response [6, 8, 25–28]. However a complete theory, which can explain the processes involved at different scales (from atomic to system scale) in contact issues, has not been yet formulated. In this context, experimental analyses with the support of numerical contact simulations can allow to discover further and relevant aspects of frictional contact phenomena arising during relative motion between elastic media. This paper presents experimental tests allowing for validating the instability contact scenario obtained numerically [19].

The first part of the paper shows the results obtained by the experimental analysis of two polycarbonate blocks in sliding motion. As a function of system parameters the same system exhibits different behaviour switching from macro stick–slip phenomena to mode coupling instability up to stable continuous sliding. A different structural response (vibrations amplitude, excited frequencies and accelerations) of the system has been observed as a function of system parameters.

The second part of the paper shows the comparison between numerical and experimental analysis as a function of same system key parameters. A contact law that considers the coefficient of friction as a function of the adherence time is accounted for in the finite element model, in order to simulate the frictional behaviour of the polycarbonate blocks.

With respect to recent literature, the presented results allow to validate experimentally the generalization of the frictional contact scenarios between two bodies in frictional contact, showing how the local contact dynamics (rupture and wave propagation) can make switch the system macroscopic frictional

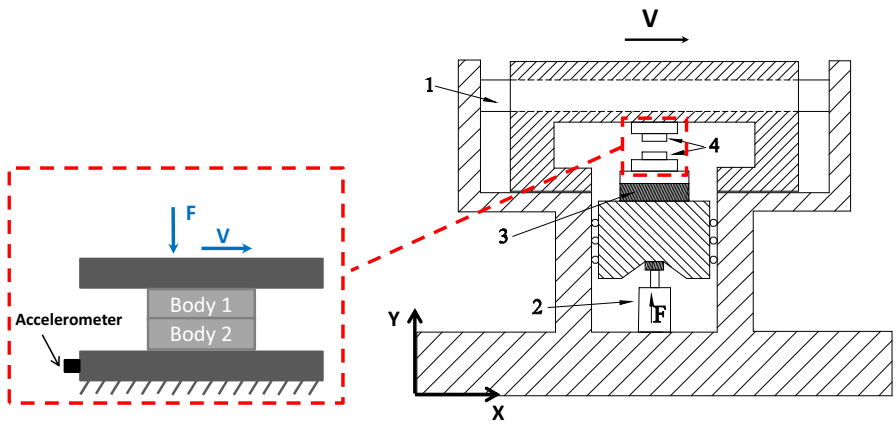

Fig. 1 A general scheme of the experimental set-up: *1* hydraulic cylinder, *2* hydraulic piston, *3* force transducer, *4* specimens of polycarbonate

Table 1 Material and geometrical properties of polycarbonate specimens

	Polycarbonate
Length (mm)	30
Width (mm)	10
Thickness (mm)	5
Density (kg/m^3)	1,190
Young modulus (GPa)	2.65
Poisson coefficient	0.4

behaviour from macroscopic stick–slip to mode coupling instability or continuous stable sliding. The correlation with numerical results allows to explain this behaviour just accounting for the local dynamics at the contact and a simple Coulomb contact law, rather than introducing "ad-hoc" contact or interface laws to match the experimental evidences.

While the numerical simulations allow for the understanding of the physical phenomena and investigating the coupling between contact and system dynamics, the experimental results allow for validating the numerical findings.

2 Experimental set-up

This section presents a description of the experimental test bench used to provide the relative motion of two elastic bodies in contact under well controlled boundary conditions.

Two blocks of polycarbonate (Fig. 1) have been used to carry out the experimental tests. The material and geometrical properties of the polycarbonate blocks are reported in the following table:

The dimensions of the specimens (Table 1) are set in order to obtain a better planarity of the two contact surfaces and a considerable average contact pressure. The contacting faces of the two blocks have been polished and each contact face has been cleaned by ethyl alcohol before of performing the tests.

The set-up (a simplify scheme is reported in Fig. 1) is rigidly linked at a seismic mass (5,000 kg). The upper specimen is fixed to the mobile part of the set-up that provides the translation displacement (along x direction) through hydraulic cylinders, controlled in position with a linear encoder. The lower specimen is bonded to the fixed part (along x) and the normal load (along y direction) is applied through a hydraulic piston, controlled in force. A tri-axial piezoelectric force transducer records the tangential and normal force both in the preload phase and during the relative motion. A piezoelectric accelerometer (Fig. 1) is positioned on the support of the lower specimen to measure the tangential acceleration during tests. In the first phase of each test, the lower and upper specimens are put in contact applying a compressive normal force F_N; afterward a constant velocity is imposed on the upper specimen to bring the blocks in frictional relative motion. The global signals, tangential force, normal forces, tangential acceleration and imposed displacement have been recorded with a sample frequency of 50 kHz by the OROS acquisition system. The translational velocity is imposed to the slider block by a linear hydraulic displacement system with high resolution in order to avoid artificial stick–slip phenomena induced by the set-up control system. The

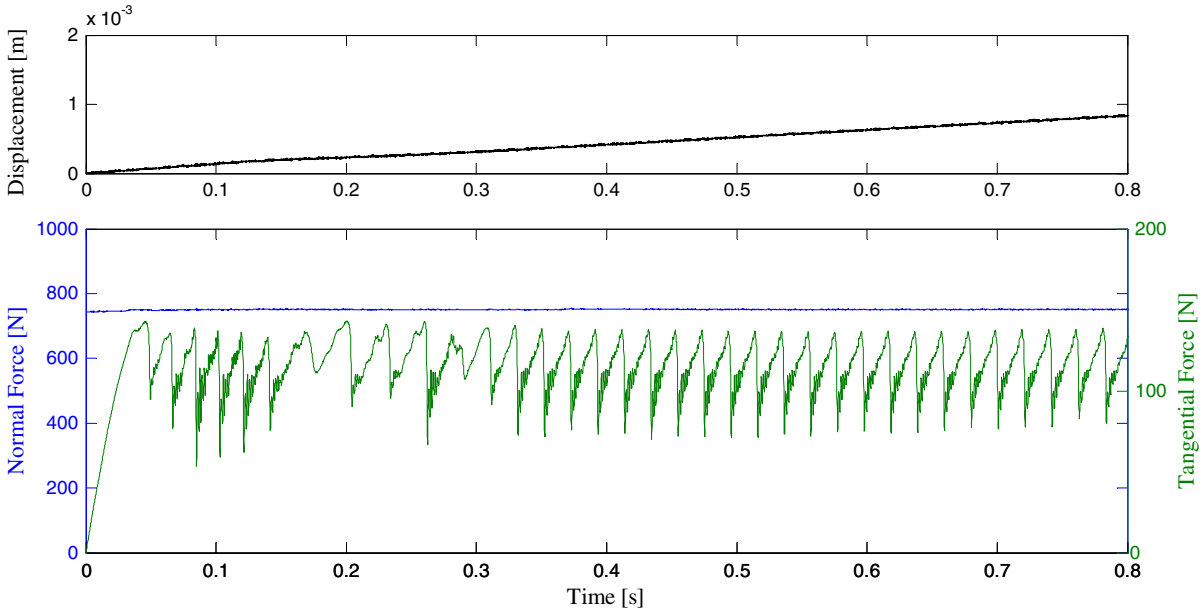

Fig. 2 Imposed displacement (*up*); normal (y direction) force and tangential (x direction) force (*down*). Experimental data obtained with the following parameters: imposed slider velocity 1 mm/s and normal load 750 N

set-up allowed imposing at the system the opportune (constant) boundary conditions in order to obtain reproducible results and to perform a comparison with numerical results.

An experimental parametrical analysis, as function of the slider velocity and the normal load, has been performed. Four different values of normal force have been tested, 150, 450, 750, 1000 N, corresponding to an average contact pressure of 1, 3, 5, 6.6 MPa respectively. For each value of the normal load, the slider velocity has been ranged between 10 mm/s and 2 μm/s with a maximum total displacement of 5 mm. This set-up allowed observing different macroscopic frictional behaviours when two simple elastic media are in relative motion under frictional contact.

3 Observation of frictional behaviours

This section presents the different macroscopic frictional behaviours observed between the two elastic bodies, when the relative translational velocity is varied. Experimental tests have been performed ranging the velocity of the upper slider block, while the normal load is fixed to 750 N in order to obtain an average contact pressure of 5 MPa. At the end of the section the effect of normal load and imposed horizontal velocity on the contact scenarios is discussed.

3.1 Macro stick–slip instability

Figure 2 shows the results for an imposed translational velocity of 1 mm/s. The blue and green curves show respectively the tangential and normal global forces recorded by the force transducer. The black curve represents the imposed displacement in order to have constant translational velocity along the x direction. First, a normal force along y direction is applied to the system in order to obtain an initial average normal pressure of 5 MPa. After this preload phase, not reported in figure, a constant velocity is imposed to the body 2 (Fig. 1).

After a first ramp due to the tangential loading phase, the curve of tangential force (Fig. 2) exhibits periodic drops and subsequent ramps along the recorded time. Each increase of the tangential force (increase of elastic energy stored in the system) is followed by a sudden drop due to the following macro-slip at the contact surface [18]. The slope of the initial tangential curve is function of the tangential stiffness of the whole system during the tangential loading

phase. During each load phase, until the tangential force reaches the maximum value, the bodies are globally still in adherence status while some contact zones can switch in sliding state before the macro-slip due to the interface rupture propagation (precursors) as shown in [6, 18, 29].

Then, a sudden macroscopic slip occurs with the consequent drop of the tangential force. The sliding of the whole interface is due to the rupture and wave generation and propagation at the contact interface [18] that produces the release of the elastic energy stored in the system during the loading (sticking) phase.

The sudden macro slip of the contact interface represents an impulsive excitation for the system and the generated vibrations, measured at the piezoelectric accelerometer (see Fig. 5a), are related to the dynamic response of the whole set-up. Figure 5b shows the spectrum of the acceleration signal for a time interval Δ_1, i.e. a time period between two macro slip, characterized by the response to the impulsive (force drops) system excitation, where the first natural frequencies (110, 600, 900, 1500, 2400 Hz) of the whole system are excited. On the other hand the spectrum in Fig. 5c is referred to time interval Δ_2 and shows a superposition of the super-harmonics of the stick–slip frequency (50 Hz) together with the excited system natural frequencies. Thus, the macroscopic frictional behaviour, characterized by periodic drops of tangential force and referred in literature as stick–slip [7], is originated by the local contact rupture propagation that excites the whole system dynamics. The propagation of the contact waves and the interaction with the structural dynamics play a key role into defining the frictional behavior of two elastic media in relative motion. This kind of frictional instability can occur in any mechanical system with frictional interfaces and it is also referred as the main mechanism at the origin of earthquakes [30].

3.2 Mode coupling instability

Increasing the driving velocity and maintaining fixed the normal force (750 N), the macroscopic frictional behaviour changes its pattern (Fig. 3). Figure 3 shows the system behaviour for an imposed translational velocity equals to 5 mm/s. After the preload phase, the translational velocity is imposed and the tangential force (green curve in Fig. 3) reaches its maximum value higher than the mean tangential force at steady state. Then, after the first macroscopic slip, the system shows large oscillations of the global frictional force around its mean constant value (green curve in Fig. 3). Furthermore the recorded acceleration highlights the typical behaviour of mode coupling instability (see Fig. 5d): a first phase (time interval Δ_1 in Fig. 5d) with an initial exponential increase of oscillations and harmonic spectrum at the unstable natural frequency followed by a second phase where the response is bounded to a limit cycle (time interval Δ_2 in Fig. 5d). The spectrum of the first phase (Fig. 5e) shows a main frequency peak, representing the fundamental harmonic at 110 Hz. The relatively low frequency of the vibrations is associated to an unstable mode of the whole experimental set-up. The spectrum in the second phase (Fig. 5f) shows the main harmonic at 110 Hz and the respective super-harmonics of the signal, due to the contact non-linearities that bound the vibration. The harmonic vibrations in Fig. 5f, induced by frictional contact forces, are typical of mode coupling instability [19, 24]. In fact, when the two bodies are in relative motion the contact forces can excite an unstable mode of the system [19] and, after an initial exponential increase of the vibration, a limit cycle is reached; the acceleration signal in Fig. 5d shows the exponential increasing until the material damping and contact non-linearities stabilize the system response. This kind of contact scenario, typically studied in brake or clutch systems, has been experimentally highlighted also here for general mechanical system under frictional contact. The same contact scenario has been analysed numerically in [19] where the interaction between local behaviour at the contact and system dynamics has been analysed as a function of the material damping.

3.3 Stable continuous sliding

Considering the same mechanical system, Fig. 4 shows its macroscopic behaviour during relative motion obtained for a translational velocity of 10 mm/s, while the normal load is fixed to 750 N. First, the tangential force reaches its maximum value, higher than the tangential force at the steady state; afterwards the entire system remains in sliding status and the frictional force stabilizes (decaying oscillations) reaching a steady value. On the other hand, the

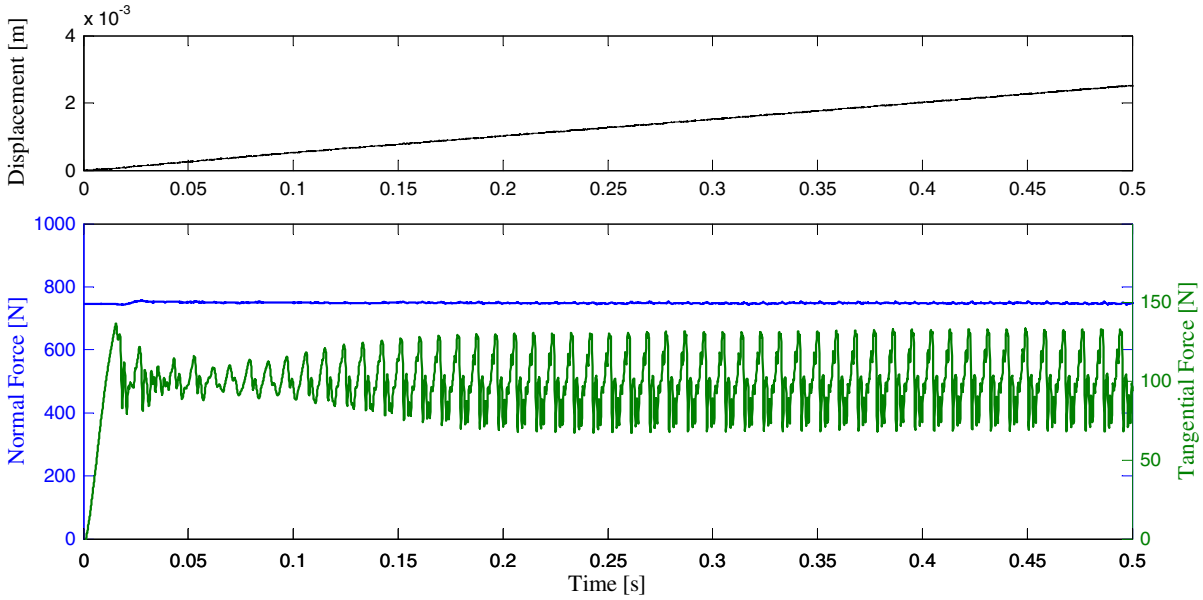

Fig. 3 Imposed displacement (*up*); normal (y direction) force and tangential (x direction) force (*down*). Experimental data obtained with the following parameters: imposed slider velocity 5 mm/s and normal load 750 N

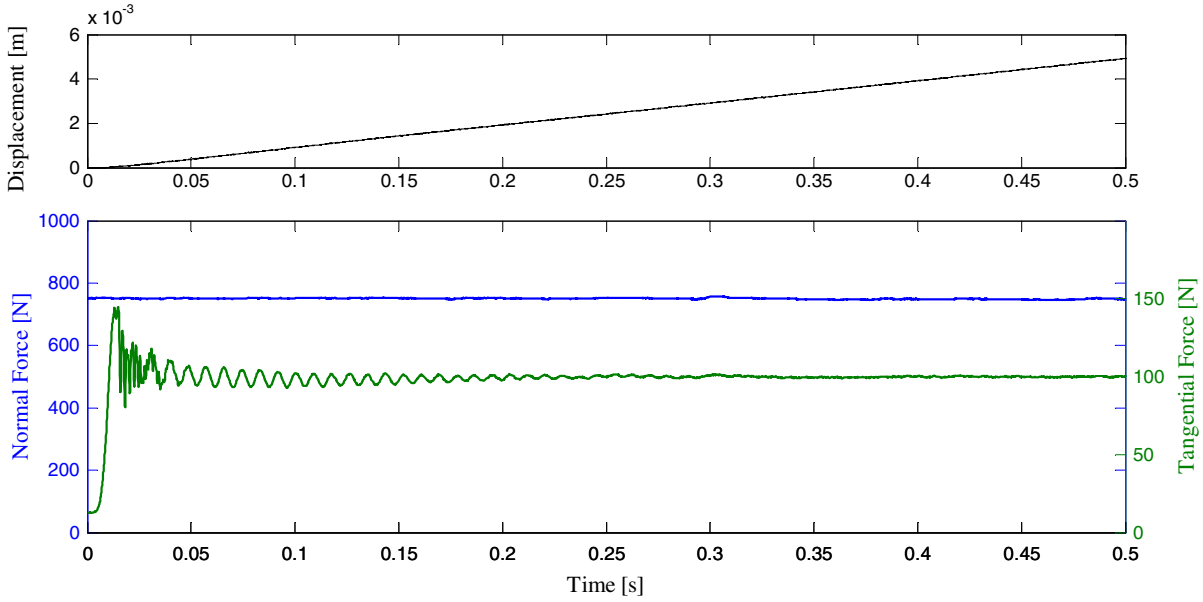

Fig. 4 Imposed displacement (*up*); normal (y direction) force and tangential (x direction) force (*down*). Experimental data obtained with the following parameters: imposed slider velocity 10 mm/s and normal load 750 N

acceleration signal in Fig. 5g shows typical decaying oscillations due to the initial drop of tangential force (Fig. 4); the spectrum of the signal in this first phase (Fig. 5h) shows how the decaying oscillations are related to the first natural frequencies of the set-up. Afterwards the system response is stable and no relevant oscillations can be observed from the recorded signal and its related spectrum (Fig. 5i).

In this case the relative motion between the two bodies of polycarbonate can be considered stable and

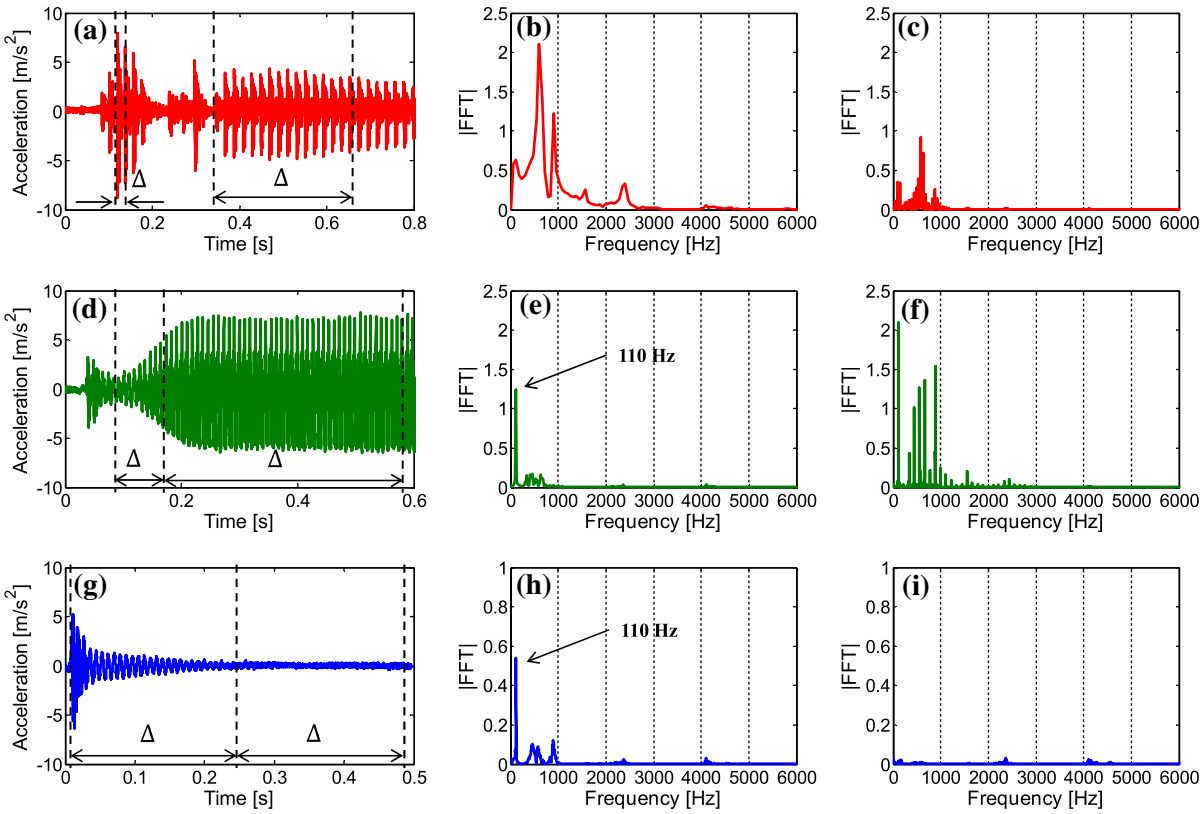

Fig. 5 Frictional instability map with normal load equal to 750 N. **a–c** Macro stick–slip instability for V = 1 mm/s; **d–f** mode coupling instability for V = 5 mm/s; **g–i** stable continuous sliding for V = 10 mm/s. Alongside each contact scenario (acceleration signals) the spectrum related to different time period Δ_1 and Δ_2 is shown

the structural dynamics of the system is not excited (not relevant oscillations), as it can be observed from the measured tangential force and acceleration.

3.4 Discussion on contact behaviours: frictional scenario map

The experimental results highlighted how a simple frictional system can exhibit different macroscopic contact scenarios (macro stick–slip, mode coupling instability, stable continuous sliding) as a function of the boundary conditions. Figure 5 shows as the frictional contact forces can excite the system dynamics differently, when increasing the imposed velocity. The macroscopic behaviour of the system can be characterized by intermittent interface motion and impulsive excitation of the system (macro stick–slip instability in Fig. 5a), continuous sliding at the interface with harmonic vibration of the system (mode coupling instability in Fig. 5d) or continuous stable sliding state (Fig. 5g). In particular, the spectrum of the tangential acceleration during the macro stick–slip scenario (Fig. 5c) highlights how the system vibration amplitude is lower with respect to the amplitude of the acceleration in the limit cycle during mode coupling instability (Fig. 5f). Furthermore, in the first case the system behaviour is characterized by intermittent interface motion, while in the second case the system can be considered in continuous sliding state with large periodical oscillations of the local contact forces, up to reach local changes in the contact status (local stick or detachment) [18, 19].

The same transition from stable continuous sliding state to macro stick–slip instability has been also observed experimentally as a function of initial normal load, ranging from 150 N (1 MPa) up to 1,000 N (6.6 MPa), maintaining fixed the imposed horizontal velocity (Fig. 6). The experimental parametrical analysis, carried out on the two blocks of polycarbonate as a function of boundary conditions allowed for drawing

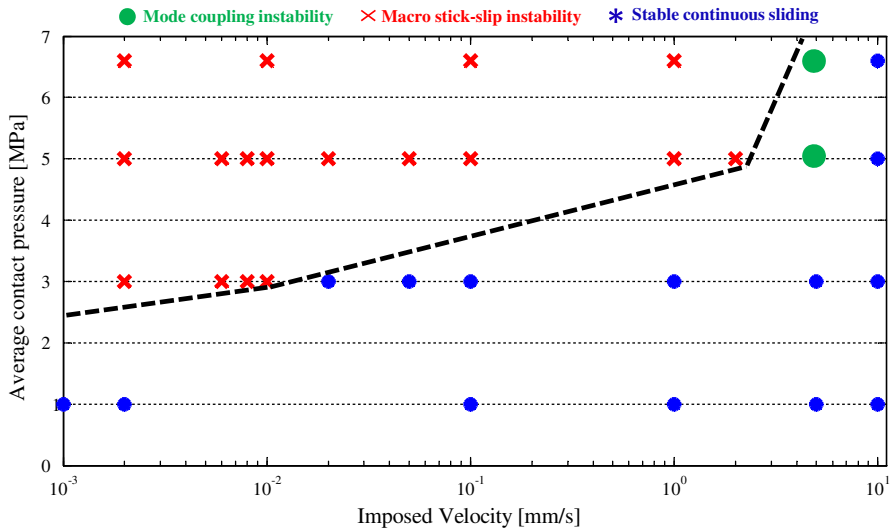

Fig. 6 Experimental map of the frictional contact scenarios as a function of translational velocity V and average contact pressure

a contact scenarios map of the system. Figure 6 highlights the role of normal load and imposed velocity into the switching from macroscopic stick–slip instability and continuous sliding behaviour with or without mode coupling instability. For low normal load (low average contact pressure) the system is characterized by stable behavior for the whole imposed velocity range (between 2 μm/s and 10 mm/s). Increasing the normal load the system starts to exhibit unstable contact behavior for relative low imposed velocity, as shown in Fig. 6. Similar maps of the frictional behavior can be drawn numerically for other system parameters, as shown in [19].

4 Comparison between experimental and numerical results

This section presents the comparison with results obtained by transient contact non-linear simulations, carried out to analyse the contact dynamics of elastic media in frictional contact. Numerical analyses have been performed in order to investigate the coupling between the local contact dynamics and the dynamic response of the whole system. The different macroscopic scenarios between elastic media under frictional contact have been obtained as a function of system parameters. A good agreement between numerical and experimental scenarios is presented, showing comparable behaviours as a function of boundary conditions (normal load and imposed velocity).

Table 2 Material and geometrical properties of the numerical model

	Body 1	Body2
Length (mm)	30	30
Width (mm)	10	10
Element number	30,000	5,590
Contact element size (mm)	0.1	0.23
Young modulus (GPa)	2.65	2.65
Density (kg/m^3)	1,190	1,190
Poisson ration	0.40	0.40
Material damping: alpha (1/s)	40	
Material damping: beta (s)	1e−7	
Simulation time step (s)	9e−9	

4.1 Finite element model: geometry and contact formulation

The 2D model (plane strain deformation) consists of two isotropic elastic finite media separated by a frictional interface (Fig. 7); at each node of the contact interface is imposed the friction law (see Sect. 4.2). The material and geometrical properties of the numerical model are listed in Table 2. A force distribution along y axis, giving a global force F, is applied at the bottom of the body 2. After the preload phase, the global normal force F is maintained constant and a translational velocity V, along the x direction, is applied at the lower edge of the body 2 to bring the system in relative

motion; the body 1 is maintained fixed at its upper side.

The explicit finite element code PLASTD [31, 32] is used to perform transient contact nonlinear simulations in order to analyse the local contact dynamics and structural response due to the system excitation by the frictional forces. This software is designed for large strains, large displacements, large rotations and non-linear contact behaviour using a forward Lagrange multiplier method for the contact between deformable bodies. The bodies are described by a four node quadrilateral elements with 2 × 2 Gauss quadrature rule and the contact algorithm uses slave nodes and target surfaces. The elementary target segments are described by two nodes and approximated by bicubic splines. A forward Lagrange multiplier method is formulated by equations of motion at time ($t_i = i\Delta t$) with the displacement conditions imposed on the slave node at time t_{i+1}:

$$\begin{cases} \mathbf{M}\ddot{\mathbf{u}}_\mathbf{i} + \mathbf{C}\underline{\mathbf{u}}_\mathbf{i} + \mathbf{K}\mathbf{u}_\mathbf{i} + \mathbf{G}_{\mathbf{i+1}}^{\mathbf{T}}\boldsymbol{\lambda}_\mathbf{i} = \mathbf{F}_\mathbf{i} \\ \mathbf{G}_{\mathbf{i+1}}\{\mathbf{X}_\mathbf{i} + \mathbf{u}_{\mathbf{i+1}} - \mathbf{u}_\mathbf{i}\} \leq 0 \end{cases} \quad (1)$$

where **M** and **K** are, respectively, symmetric and positively defined matrices of mass and stiffness of the system; **C** is the Rayleigh proportional damping matrix where α is the mass damping coefficient and β is the stiffness damping coefficient:

$$[\mathbf{C}] = \boldsymbol{\alpha}[\mathbf{M}] + \boldsymbol{\beta}[\mathbf{K}] \quad (2)$$

X_i is the coordinate vector at time t_i. u, $\dot{u}$, $\ddot{u}$ are respectively the vectors of nodal displacements, nodal velocities and accelerations. F_i is the vector of external forces. The contact algorithm uses slave nodes and target surfaces. $\lambda_i = [\lambda_n \lambda_t]^T$ contains respectively normal and tangential contact forces acting on the nodes at the contact surface. $G_i^T = [G_n^T G_t^T]$ is the global matrix of the displacement conditions ensuring non-penetration condition and the contact law at the boundaries in contact. The formulation is discretized temporally by using an explicit Newmark scheme. The explicit Newmark scheme coupled with forward Lagrange multiplier method allows to satisfy more precisely the contact conditions. Furthermore explicit method allows for better solve problems involving impact and sliding with friction [32] and fast phenomena such wave and rupture propagations at the contact.

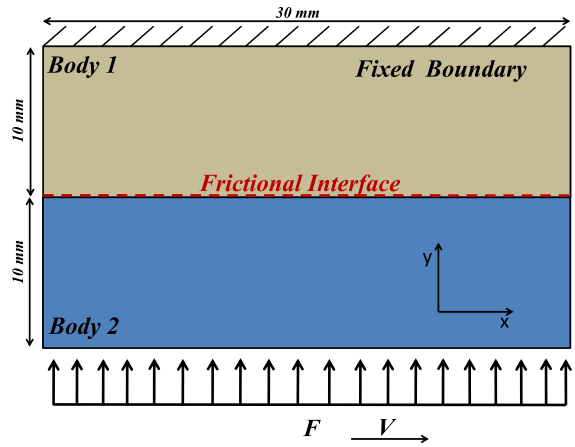

Fig. 7 Geometry and boundary conditions of the numerical contact model

Because of the relative thickness of the bodies in contact, a plane strain deformation model has been used in order to have reasonable computational time, which is today the main limit into solving 3D transient non-linear contact simulations.

4.2 Definition of the friction law

In the present finite element model the coefficient of friction is not assumed to be a constant value (Coulomb-Amounts friction law). In fact, the experimental frictional analysis, performed on polycarbonate materials, highlighted as the macroscopic friction coefficient shows relevant variations as a function of imposed boundary conditions.

Based on frictional observations, a more realistic friction model has been implemented in the code. In particular, the value of the friction coefficient between the two surfaces of polycarbonate has been observed to be a function of the sticking (adherence) time between the two surfaces; this behaviour is probably due to the molecular reaction at the interface that increase the static friction coefficient with the increase of the adherence time.

Then, the implemented friction law describes the local friction coefficient (imposed at each contact node of the model) as a function of adherence time. The definition of a reliable law of friction has been derived as a function of the experimental tests carried out on the polycarbonate blocks (Fig. 8).

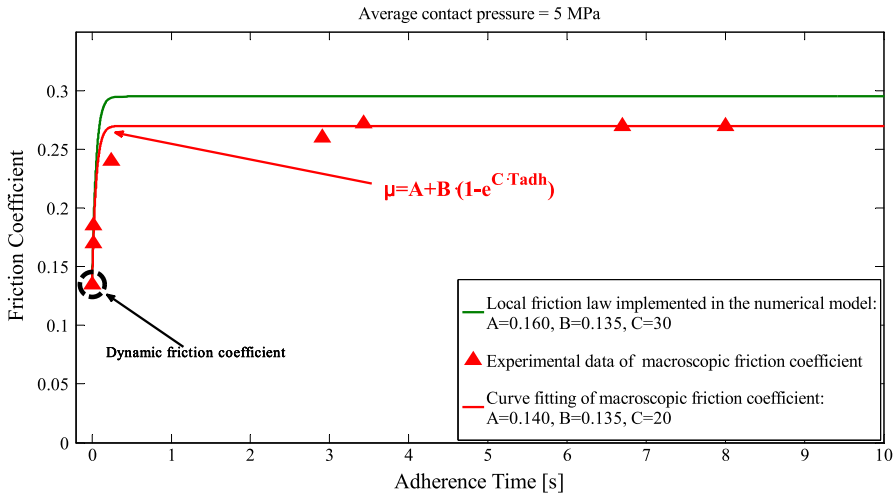

Fig. 8 Curve fitting of friction contact law used into the finite element model for an average contact pressure of 5 MPa

Figure 8 shows the curve fitting of experimental points of the macroscopic friction coefficient, obtained considering the performed experimental tests at an average pressure of 5 MPa. The experimental data (red triangles in Fig. 8) represents the static friction coefficient calculated as the maximum ratio between tangential force and normal force recorded during the macro stick–slip instability behaviour for a fixed imposed velocity. At each experimental point in Fig. 8 has been associated the adherence time calculated by the period of the stick–slip events for each considered imposed velocity. This assumption has been considered under the hypothesis that between two following macro slip, observed experimentally, the contact interface stays in adherence (stick phase).

The point marked by a black dashed circle is the dynamic friction coefficient experimentally estimated as the ration between the tangential force and normal load in the case of stable continuous sliding (Fig. 6), equivalent to a nil adherence time.

The curve fitting of the experimental results led to obtain an analytical curve of the friction contact law able to be implemented in the numerical contact model:

$$\mu(t_{adh}) = A + B \cdot \left(1 - e^{-C \cdot t_{adh}}\right) \tag{3}$$

where the t_{adh} represents the adherence time; A + B is the static friction coefficient; A is the dynamic friction coefficient defined precisely for $t_{adh} = 0$; C is the parameter influencing the increase or decrease of friction coefficient in the first interval time of the friction law as shown in Fig. 8.

The experimental analysis of the friction coefficient highlighted some important variations of static coefficient for short adherence times and a stabilization of friction curve for high time of adherence, as shown in Fig. 8. This kind of friction law wants, in a simple way, to account for the complex mechanisms at the contact interface such as adhesion, physical and chemical actions, and viscoelastic deformations of asperities that occur at the interface. These mechanisms play a key role into define the local frictional contact behaviour, but at the same time they are difficult to be implemented in a numerical model [3, 33]. Nevertheless, the experimental macroscopic measurements of the contact forces allow for defining reliable parameters of the friction law (Eq. 3) to be representative, as much as possible, of the local physics at the interface.

The same behaviour of the macroscopic friction coefficient, shown in Fig. 8, has been also observed for the average normal pressure of 3 MPa and 6.6 MPa; then, a similar friction law has been estimated for each values of the contact pressure, modifying the parameters A, B, C as a function of the experimental points (Table 3). The difference on the friction, observed experimentally as a function of average pressure, could be due to the effects of the real contact pressure on the surface mechanisms listed above.

It has been also observed that determining the static friction coefficient from the time evolution of tangential force underestimates the real value of static friction coefficient [19, 29, 34]; in fact the

difference between apparent (macroscopic) and real (local) static friction coefficient is due to the local contact dynamics at the frictional interface, which lead to have macro-sliding for a tangential force lower than the upper limit imposed by the friction coefficient, as explained in the literature [18, 35]. After these considerations, in order to perform the comparison between experimental and numerical results obtained by the nonlinear transient analysis, the values of static friction coefficient has been increased of 15 % as showed by the friction law reported in Fig. 8 (green curve).

Table 3 Parameters of the friction law implemented in the numerical model

Average contact pressure (MPa)	A	B	C	Max static friction coefficient (A + B)	Dynamic friction coefficient (B)
3	0.14	0.20	30	0.34	0.20
5	0.16	0.135	30	0.295	0.135
6.6	0.14	0.125	35	0.265	0.125

4.3 Effect of imposed boundary conditions

This section presents a comparison between the experimental tests and the numerical results carried out by means of transient non-linear simulations. The effect of the boundary conditions, horizontal velocity and normal force (average contact pressure), has been numerically investigated considering a 2D plane strain model, for which the only non-linearity accounted for is the contact behaviour (see Sect. 4.2). The black curve in Fig. 9 shows the displacement imposed at the lower edge of the model in order to obtain a steady velocity of 1 mm/s; like in the experimental tests, before applying the constant translational velocity, a preload phase has been realized to bring the two blocks in contact with average normal pressure of 7.6 MPa. The simulation results highlight how the system behaviour is characterized by stick–slip phenomena (Fig. 9). After a first linear growth, the tangential contact force exhibits repetitive fluctuations (ramps and sudden drops). The released of elastic energy during the drops produces strong vibrations into the system. The same contact scenario characterized by macro stick–slip has been revealed experimentally for

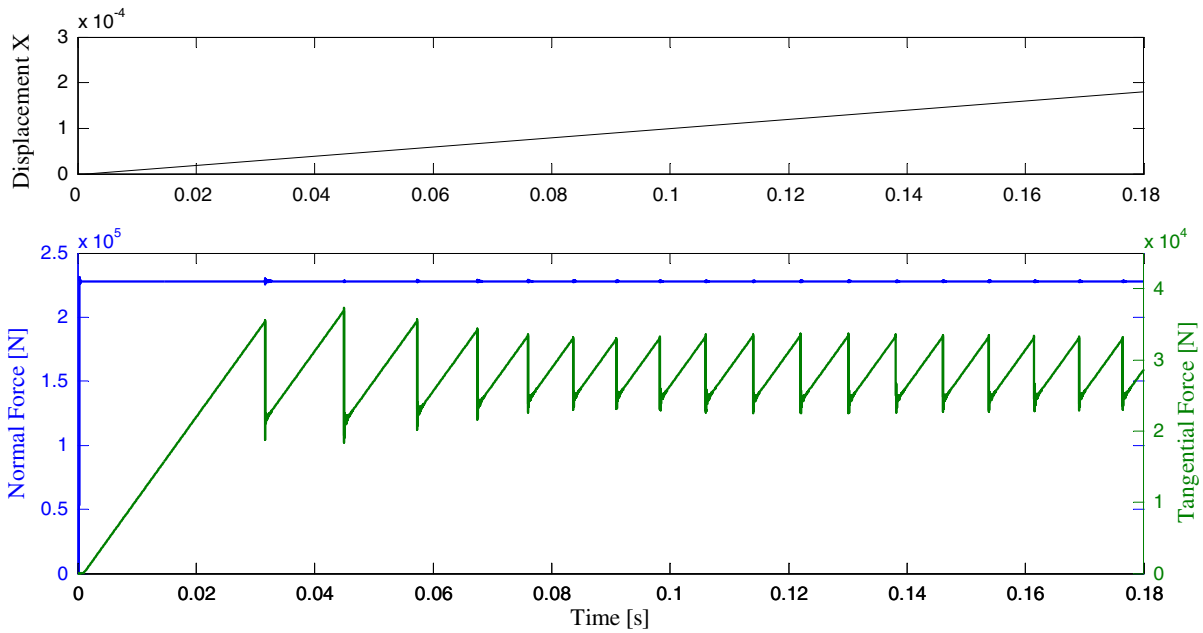

Fig. 9 Imposed displacement at lower edge of body 2 (*up*); normal force (along y direction) and tangential force (x direction) measured numerically at the *upper edge* of the body 1. Imposed boundary condition: horizontal velocity V = 1 mm/s and average contact pressure 7.6 MPa

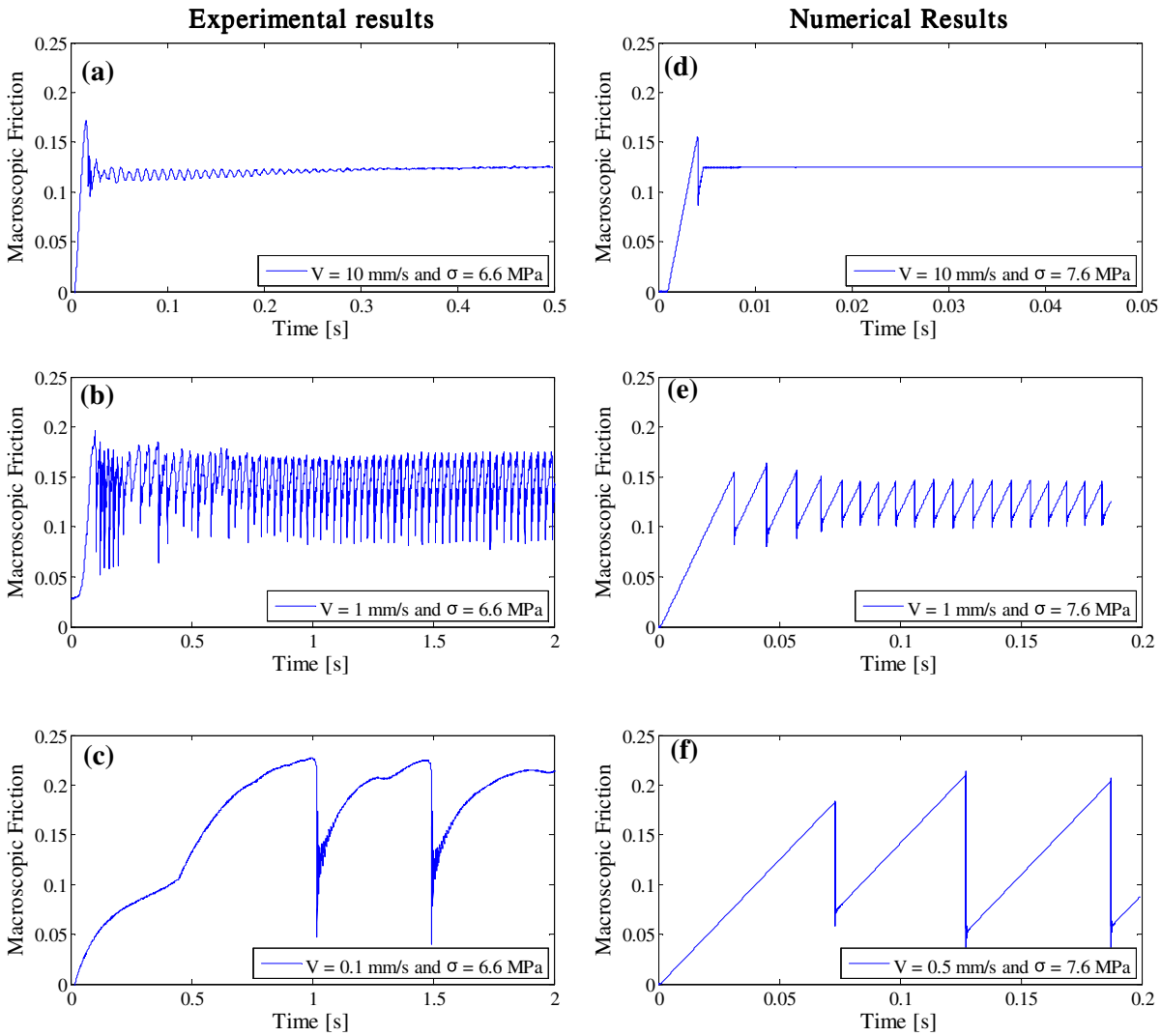

Fig. 10 Comparison between experimental and numerical results on transition from stable continuous sliding to macro stick–slip instability as a function of imposed velocity V. **a–c** Experimental results ranging the imposed velocity between 10 mm/s to 0.1 mm/s and average contact pressure of 6.6 MPa. **d–f** Numerical results ranging the imposed velocity between 10 and 0.5 mm/s and average contact pressure of 7.6 MPa

an imposed velocity of 1 mm/s and average pressure of 6.6 MPa (Fig. 2).

Figure 10 shows the effect of the imposed horizontal velocity, both experimentally and numerically, on the macroscopic frictional behaviour. The macroscopic friction coefficient along the time has been calculated as the ratio between the total tangential force and normal force measured at the boundaries for both numerical and experimental samples. Ranging the imposed velocity from 10 to 1 mm/s and maintaining fixed the normal force (average pressure of 7.6 MPa) the behaviour of the numerical system changes its pattern (Fig. 10, right) as shown also in the experimental measurements (Fig. 10, left). For a translational velocity of 10 mm/s and an average contact pressure of 7.6 MPa the numerical model exhibits a typical stable continuous sliding behaviour (Fig. 10d) as observed experimentally for the same value of the sliding velocity and an average pressure of 6.6 MPa (Fig. 10a). The friction coefficient shows a linear increase until it reaches the maximum value and, after a sudden drop due to the released elastic

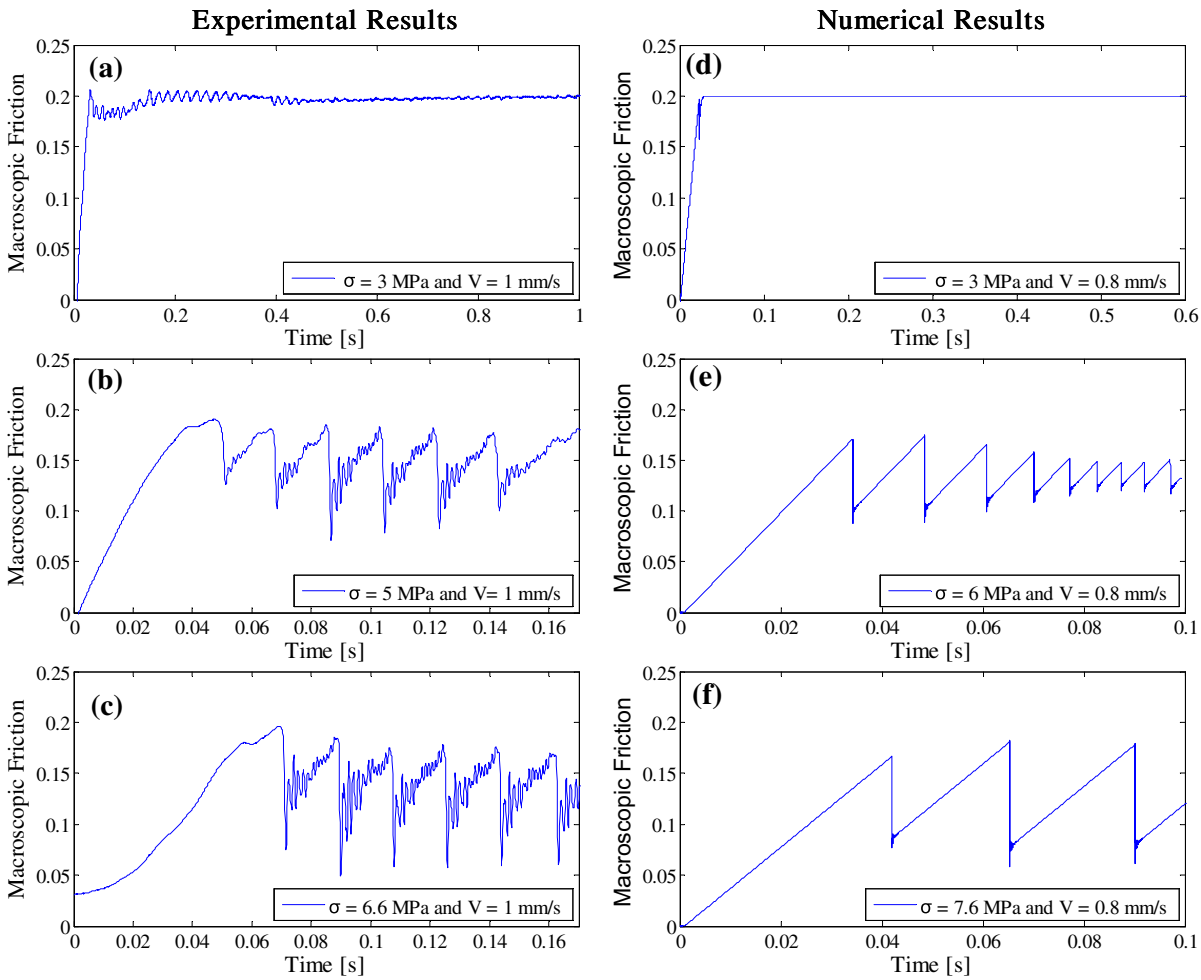

Fig. 11 Comparison between experimental and numerical results on transition from stable continuous sliding to macro stick–slip instability as a function of average contact pressure. **a–c** Experimental results ranging the average contact pressure between 3 and 6.6 MPa and impose velocity of 1 mm/s. **d–f** Experimental results ranging the average contact pressure between 3.5 and 7.6 MPa and imposed velocity of 0.8 mm/s

energy, its value stays constant. The initial drop in the friction coefficient (related to tangential force drop) produces an excitation that leads to decaying oscillations of the system (Fig. 10d). After this first phase of transition from adherence to sliding state of the whole surface, the friction coefficient stabilises itself reaching a steady value of 0.125, like in the experimental test (Fig. 10a).

Decreasing the horizontal imposed velocity, both experimentally and numerically, the macroscopic behaviour changes completely its pattern (Fig. 10b, e). The drops of the tangential force along the time produce periodic fluctuations in the macroscopic friction curve, as shown in Fig. 10 for an imposed velocity of 1 mm/s. Continuing to decrease the imposed velocity for values lower than 1 mm/s and maintaining fixed the average normal pressure the response of the system doesn't change its pattern: the macroscopic contact scenarios is always characterized by macro stick–slip phenomena (Fig. 10c, f). However Fig. 10c, f show that, both numerically and experimentally, the amplitude of the drops of the macroscopic friction and the time period of stick–slip events increase when the imposed velocity is reduced.

Figure 11 shows the main effect into defining the macroscopic response of the system when the normal force (average contact pressure) is varied between 3 and 6.6 MPa for experimental measurements and

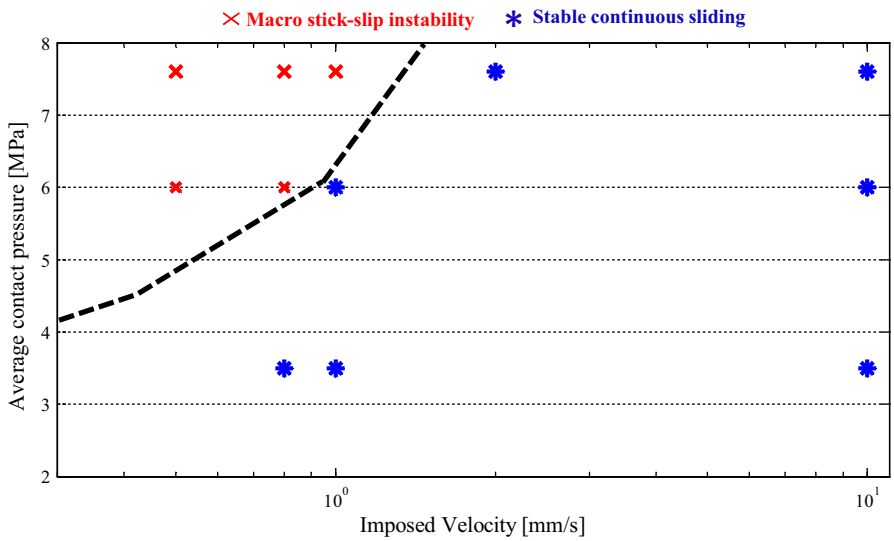

Fig. 12 Numerical map of the frictional contact scenarios as a function of translational velocity V and average contact pressure

between 3.5 and 7.6 MPa for the numerical simulations, while the translational velocity is maintained fixed. For low contact pressure the system is characterized by a stable continuous sliding; the friction coefficient increases reaching the constant value of 0.20 with not relevant oscillations of the system (Fig. 11a, d). On the other hand, increasing the contact pressure, the system (numerically and experimentally) switches from stable sliding to macro-stick slip instability, showing several variations (drops) in the macroscopic friction coefficient along the time. The sudden drop of tangential force produces a strong system vibration with a decaying behaviour during each ramp, immediately after the friction drop.

For both experimental and numerical results, when increasing further the contact pressure, the amplitude of the drops in the friction coefficient increases reaching a lower limit of macroscopic friction around 0.05 due to the important released of elastic energy stored during the ramp.

It should be noticed that the decaying vibrations excited experimentally after each force drop present low frequency components (mainly at about 110 Hz) due to the dynamic response of the modes of the whole experimental set-up; in the numerical curves only decaying oscillations at higher frequencies can be observed and are related to the dynamics response of the modes of vibrations of the two block of polycarbonate.

Similarly, the differences in term of amplitude and period of stick–slip events between experimental and numerical tests are due to the fact that the numerical model simulates the dynamics of two polycarbonate blocks without accounting for the stiffness and dynamics of the whole experimental set-up. On the other hand the experimental setup is composed by auxiliary parts that can't allow defining an exact quantitative comparison between experimental and numerical results.

The main differences, due to the lack in modelling of the whole set-up, is the different tangential stiffness of the numerical and experimental systems, which brings to a different slope of the tangential force and consequently to different values of the time period between successive stick–slip events.

Another not negligible difference is the presence of the set-up modes at lower frequencies which brings to the low frequency oscillations recorded in the experimental test and not observable in the numerical curves.

Nevertheless, the effect of the impose boundary conditions recovered by means of the numerical simulations, exhibits a good agreement with the experimental results. The experimental transition from stable continuous sliding to macroscopic stick–slip for the polycarbonate blocks has been obtained for the same trend of the boundary conditions.

The performed simulations allowed to draw a numerical map of possible contact scenarios (Fig. 12), showing the good qualitative agreement with the experimental map in Fig. 6. The missing of the mode coupling instabilities in the numerical map is

due to the missing of the unstable mode of the whole set-up at 110 Hz. In fact, the complex eigenvalue analysis [19] of the numerical model of the polycarbonate blocks alone doesn't predict unstable system modes. The unstable mode recovered experimentally (see Sect. 3.2) is a lower frequency mode of the set-up, which is not modelled in the numerical analysis.

Moreover, the numerical map of the instability scenarios wants to give just the trend of the frictional scenarios as a function of the system parameters, as showed as well in [19] as a function of the material damping. In fact, the effect of all the system parameters are deeply interdependent and the boundary of these maps, calculated for a given system configuration, can vary as a function of the other system parameters.

5 Conclusions and perspectives

Contact frictional scenarios of two media in relative displacement have been investigated both by experimental tests and numerical simulations. The tests performed by the experimental set-up highlight the complex phenomena arising when two media are in frictional sliding. The same system with respect to different boundary conditions, such as imposed horizontal velocity or average contact pressure, switches its macroscopic frictional behaviour from macro stick–slip instability to mode coupling instability with harmonic vibrations, up to stable continuous sliding. A frictional scenario map, found numerically as a function of the material damping in [19], has been here drawn experimentally and numerically as a function of the boundary conditions.

The mode coupling contact instability, investigated mostly in brake squeal, has been highlighted here for two general elastic bodies in frictional relative motion. Experimental tests confirms how the macroscopic response of a simple elastic system with frictional interface is mainly influenced by local frictional dynamics (propagation of contact waves and rupture fronts) and conversely [18].

From the experimental data obtained by frictional tests on polycarbonate, an appropriate friction law with adherence time dependence has been defined. Non-linear transient simulations highlighted the same experimental transition range from stable sliding to macroscopic stick–slip as a function of the key parameters. The presented numerical nonlinear model, in which only the contact nonlinearities have been considered, confirms a good agreement with the macroscopic frictional behaviour obtained by the experiments.

The numerical simulations, validated here by the experimental results, allows for investigating the coupling between the local dynamics (rupture and wave nucleation and propagation) and the dynamic response of the system (modes of vibrations). This interaction is at the origin of the selection between the possible macroscopic frictional behaviour of the system [19, 20].

In future works experimental parametrical analyses will be performed in order to investigate the role of other key parameters such as material properties, surface roughness and other boundary conditions. Nowadays, the measurement of the local dynamics at the contact is one of the main challenges. At the same time a further numerical investigation is being developed to have a more quantitative comparison by adding the stiffness and mass of the experimental set-up in the numerical model.

References

1. Andreaus U, Casini P (2001) Dynamics of friction oscillators excited by a moving base and/or driving force. J Sound Vib 245:685–699
2. Hoffmann N, Fischer M, Allgaier R, Gaul L (2002) A minimal model for studying properties of the mode-coupling type instability in friction induced oscillations. Mech Res Commun 29:197–205
3. Renouf M, Cao HP, Nhu VH (2011) Multiphysical modeling of third-body rheology. Tribol Int 44:417–425
4. Andreaus U, Casini P (2002) Friction oscillator excited by moving base and colliding with a rigid or deformable obstacle. Int J Non-Linear Mech 37:117–133
5. D'Annibale F, Luongo A (2013) A damage constitutive model for sliding friction coupled to wear. Contin Mech Thermodyn 25:503–522
6. Rubinstein SM, Cohen G, Fineberg J (2007) Dynamics of precursors to frictional sliding. Phys Rev Lett 98:226103
7. Voisin C, Renard F, Grasso J-R (2007) Long term friction: from stick–slip to stable sliding. Geophys Res Lett 34:L13301
8. Rubinstein SM, Cohen G, Fineberg J (2004) Detachment fronts and the onset of dynamic friction. Nature 430:1005–1009
9. Rubinstein SM, Cohen G, Fineberg J (2009) Visualizing stick–slip: experimental observations of processes governing the nucleation of frictional sliding. J Phys D 42:214016

10. Hervé B, Sinou JJ, Mahé H, Jezequel L (2008) Analysis of squeal noise and mode coupling instabilities including damping and gyroscopic effects. Eur J Mech-A 27:141–160
11. Ouyang H, Nack W, Yuan Y, Chen F (2005) Numerical analysis of automotive disc brake squeal: a review. Int J Veh Noise Vib 1:207–231
12. Sinou JJ (2010) Transient non-linear dynamic analysis of automotive disc brake squeal—on the need to consider both stability and non-linear analysis. Mech Res Commun 37:96–105
13. Dezi M, Forte P, Frendo F (2014) Motorcycle brake squeal: experimental and numerical investigation on a case study. Meccanica 49:1011–1021
14. Weiss C, Gdaniec P, Hoffmann NP, Hothan A, Huber G, Morlock MM (2010) Squeak in hip endoprosthesis systems: an experimental study and a numerical technique to analyze design variants. Med Eng Phys 32:604–609
15. Heckl MA, Abrahams ID (2000) Curve squeal of train wheels, part 1: mathematical model for its generation. J Sound Vib 229:669–693
16. Goodman R, Sundaram PN (1978) Fault and system stiffnesses and stick–slip phenomena. Pure Appl Geophys 116:873–887
17. Shi Z, Ben-Zion Y (2006) Dynamic rupture on a bimaterial interface governed by slip-weakening friction. Geophys J Int 165:469–484
18. Di Bartolomeo M, Massi F, Baillet L, Culla A, Fregolent A, Berthier Y (2012) Wave and rupture propagation at frictional bimaterial sliding interfaces: from local to global dynamics, from stick–slip to continuous sliding. Tribol Int 52:117–131
19. Tonazzi D, Massi F, Culla A, Baillet L, Fregolent A, Berthier Y (2013) Instability scenarios between elastic media under frictional contact. Mech Syst Signal Process 40:754–766
20. Di Bartolomeo M, Meziane A, Massi F, Baillet L, Fregolent A (2010) Dynamic rupture at a frictional interface between dissimilar materials with asperities. Tribol Int 43:1620–1630
21. Radiguet M, Kammer DS, Gillet P, Molinari J-F (2013) Survival of heterogeneous stress distributions created by precursory slip at frictional interfaces. Phys Rev Lett 111:164302
22. Adams GG (1998) Steady sliding of two elastic half-spaces with friction reduction due to interface stick–slip. J Appl Mech 65:470–475
23. Adams GG, Nosonovsky M (2001) Elastic waves induced by the frictional sliding of two elastic half-spaces. In: Dowson D, Priest M, Dalmaz G (eds) Tribology series, vol 39. Elsevier, Amsterdam, pp 47–54
24. Massi F, Baillet L, Giannini O, Sestieri A (2007) Brake squeal: linear and nonlinear numerical approaches. Mech Syst Signal Process 21:2374–2393
25. Massi F, Rocchi J, Culla A, Berthier Y (2010) Coupling system dynamics and contact behaviour: modelling bearings subjected to environmental induced vibrations and 'false brinelling' degradation. Mech Syst Signal Process 24:1068–1080
26. Magnier V, Brunel JF, Dufrénoy P (2014) Impact of contact stiffness heterogeneities on friction-induced vibration. Int J Solids Struct 51:1662–1669
27. Meziane A, D'Errico S, Baillet L, Laulagnet B (2007) Instabilities generated by friction in a pad–disc system during the braking process. Tribol Int 40:1127–1136
28. Meziane A, Baillet L, Laulagnet B (2010) Experimental and numerical investigation of friction-induced vibration of a beam-on-beam in contact with friction. Appl Acoust 71:843–853
29. Maegawa S, Suzuki A, Nakano K (2010) Precursors of global slip in a longitudinal line contact under non-uniform normal loading. Tribol Lett 38:313–323
30. Nielsen S, Taddeucci J, Vinciguerra S (2010) Experimental observation of stick–slip instability fronts. Geophys J Int 180:697–702
31. Baillet L, Sassi T (2002) Finite element method with Lagrange multipliers for contact problems with friction. CR Math 334:917–922
32. Carpenter NJ, Taylor RL, Katona MG (1991) Lagrange constraints for transient finite element surface contact. Int J Numer Meth Eng 32:103–128
33. Renouf M, Massi F, Fillot N, Saulot A (2011) Numerical tribology of a dry contact. Tribol Int 44:834–844
34. Ben-David O, Fineberg J (2011) Static friction coefficient is not a material constant. Phys Rev Lett 106:254301
35. Baillet L, Link V, D'errico S, Berthier Y (2005) Influence of sliding contact local dynamics on macroscopic friction coefficient variation. In: Elemént RED (ed.), vol. 14/2-3, pp 305–321.